

Jacutingaite-family: a class of topological materials

F. Crasto de Lima,^{1,*} R. H. Miwa,^{2,†} and A. Fazzio^{1,‡}

¹*Brazilian Nanotechnology National Laboratory CNPEM,
C.P. 6192, 13083-970, Campinas, SP, Brazil*

²*Instituto de Física, Universidade Federal de Uberlândia,
C.P. 593, 38400-902, Uberlândia, MG, Brazil*

(Dated: November 2, 2020)

Jacutingaite, a recently discovered Brazilian naturally occurring mineral, has shown to be the first experimental realization of the Kane-Mele topological model. In this letter we have unveiled a class of materials M_2NX_3 ($M=\text{Ni, Pt, Pd}$; $N=\text{Zn, Cd, Hg}$; and $X=\text{S, Se, Te}$), sharing jacutingaite's key features, i.e., high stability, and topological phase. By employing *first-principles* calculations we extensively characterize the energetic stability of this class while showing a common occurrence of the Kane-Mele topological phase. Here we found Pt-based materials surpassing jacutingaite's impressive topological gap and lower exfoliation barrier while retaining its stability.

The spin-orbit coupling (SOC) in condensed matter is accountable for the rise of many phenomena. For instance, topological phases [1], Rashba states [2], exotic spin-textures [3], magnetic anisotropy [4], spin-orbit torque transfer [5] to cite a few. Since the successful synthesis of graphene [6], 2D materials with sizeable SOC have been pursued as a platform for designing new electronic/spintronic devices [7–9], as well as the discovery and confirmation of new physical phenomena. For instance, two-dimensional hexagonal lattices and SOC are the key ingredients to the manifestation of the quantum spin Hall (QSH) state as predicted by Kane and Mele [10].

Indeed, recent research addressing topological phases in low dimensional systems has boosted the search for new two dimensional materials with large SOC, for instance, the 2D MXenes [11, 12], and Bi-based systems [13–15]. Other strategies have been proposed based on the incorporation of adatoms [16–21] and proximity effects [22–24] in order to strengthen the spin-orbit effects. However, most of these routes face a sort of difficulties, namely (i) structural metastability, (ii) stability against environment conditions (for instance, oxidation processes), (iii) difficulties for the experimental realization, (iv) lost of 2D character due to the electronic interaction with a given substrate. Thus, new 2D materials with large SOC, that overcomes the hindrances above, are still quite desirable.

Jacutingaite (Pt_2HgSe_3), a naturally occurring mineral, discovered in Brazil by Cabral *et al.* [25] in 2008, is gaining attention in the last few years. The large SOC and the honeycomb structure of Hg atoms make jacutingaite, in its monolayer form, a place for the manifestation of the Kane-Mele topological phase [26]; whereas in its bulk form it has been predicted to host dual topology, being a weak topological insulator and a topological crystalline insulator [27–29]. Both topological phases, namely Kane-Mele in monolayer and dual in bulk Pt_2HgSe_3 , have been experimentally observed through scanning tunneling microscopy (STM) [30] and angle-resolved photoemission (ARPES) [31] measurements. Its atomic struc-

ture [Fig. 1(a)] can be viewed as the transition metal dichalcogenide (TMD) PtSe_2 with 1T structural phase, where 1/4 of the chalcogenides are replaced by Hg. Besides being a natural occurring mineral, which indicates its stability in geological pressures and temperatures, Pt_2HgSe_3 has been experimentally synthesized [30–33], as well as its counterpart Pd based jacutingaite like structure, Pd_2HgSe_3 [34]. Those findings suggest that further combinations of 1T TMD host with high SOC elements may result in novel quantum spin Hall insulators based on jacutingaite like 2D structures.

In this letter, we unveil a large class of highly stable materials hosting QSH and Z_2 metallic phases based on the Kane-Mele model. We employ density functional theory (DFT) simulations [35] of the structural and electronic properties of M_2NX_3 compounds with $M=\text{Ni, Pd, Pt}$; $N=\text{Zn, Cd, Hg}$; and $X=\text{S, Se, Te}$. Throughout the extensive analysis of phase diagrams based on MNX compounds, we present a well-grounded prediction of the energetic stability of jacutingaite like M_2NX_3 structures. Electronic structure calculations reveal the emergence of topological phases, with SOC induced (non-trivial) band gaps surpassing the one of jacutingaite. Further topological characterization reveals trivial \rightarrow non-trivial transition as a function of the chemical composition, $X=\text{S} \rightarrow \text{Te}$. Finally, addressing the design of nanodevices, we have examined some key features of these jacutingaite like structures, namely the stability/behavior of the (i) topological gap as a function of the mechanical strain, and the (ii) work function for the different M_2NX_3 combination.

As shown in Fig. 1(a), the M_2NX_3 jacutingaite like share the same backbone geometry of the 1T TMDs (MX_2), where the chalcogenide atoms (X) are partially replaced by transition metals (N), $MX_2 \rightarrow M_2NX_3$, resulting in buckled $N-M-N$ bonds. The N atoms form triangular lattices on the opposite sides of the MX_2 host, which in turn are rotated by 60 degrees with respect to each other, giving rise to a buckled hexagonal lattice. At the equilibrium geometry, the lattice constants

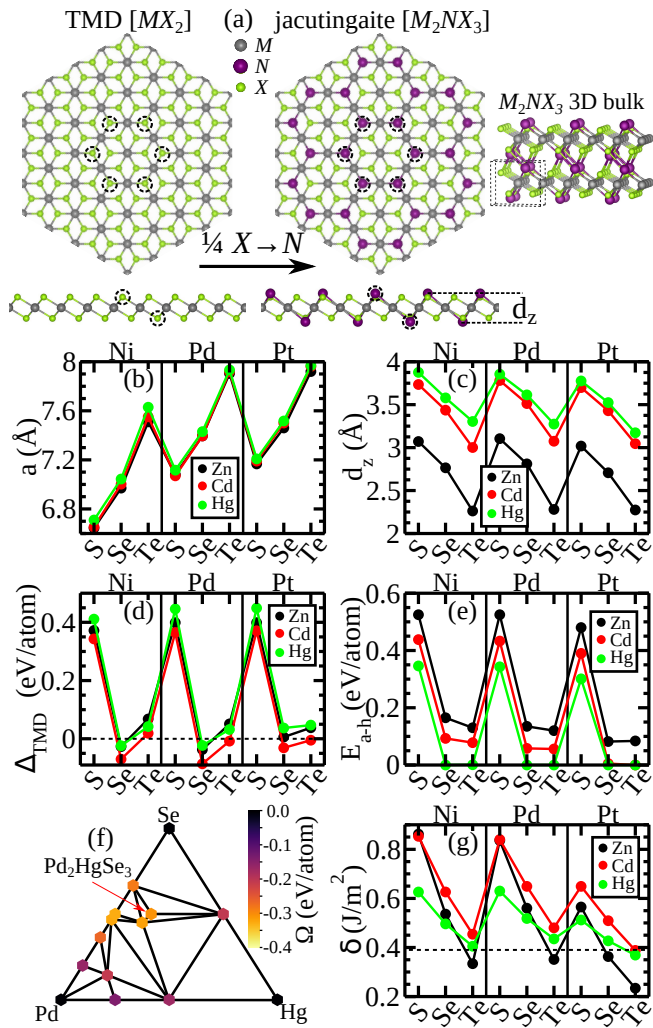


FIG. 1. (a) 2D TMD (MX_2) and 2D/3D M_2NX_3 atomic structure, (b) lattice parameter, (c) bucking distance, (d) formation energy comparison between the TMD and M_2NX_3 , (e) ternary MNX energy above hull for M_2NX_3 , (f) convex hull for Pd_2HgSe_3 and (g) cleavage energy with the dashed line indicating the graphite cleavage barrier.

of the M_2NX_3 structures are practically independent of the transition metal, i.e. nearly the same as those of the hosts (MX_2). For instance, the equilibrium lattice constants of Pt_2NSe_3 , for $N = Zn, Cd,$ and Hg , differ by less than 0.9%, compared with that of 1T $PtSe_2$. Such independence is due to the $N-M-N$ buckled structure [Fig. 1(a)] acting as a source of strain relief induced by the foreign (N) atom. As shown in Fig. 1(c), the vertical buckling (d_z) of the $N-M-N$ bonds present larger (lower) values for $X=S$ (Te).

The energetic stability of the jacutingaite like structures can be examined by comparing the formation energy of M_2NX_3 with the one of its respective (energetically stable) MX_2 host, $\Delta_{TMD} = \Omega[M_2NX_3] - \Omega[MX_2]$, Fig. 1(d). Here the formation energy is given by a total

energy difference between the compound x final system ($E[x]$), and the upper limit of the chemical potentials of its isolated compounds (μ_i^{bulk}), namely,

$$\Omega[x] = E[x] - \sum_i n_i \mu_i^{bulk},$$

where n_i indicates its number of atoms of the specie $i=M, N,$ and X . Our Δ_{TMD} results reveal that the jacutingaite like structures is quite likely to occur for $X=Se$ and Te . Here, we found negative values of Δ_{TMD} for the former, while for $X=Te$ it increases by less than 0.1 eV/atom, Fig. 1(d). Meanwhile, for $X=S$ the M_2NX_3 structure is less stable than it hosts by about 0.4 eV/atom.

Further structural stability of the jacutingaite like M_2NX_3 structures has been examined through convex energy hull analysis, comparing their formation energies (Ω) with other MNX ternary phases extracted from the Materials Project database [36–38]. We found M_2NX_3 compounds being a node point in the convex hull (zero energy above convex hull, $E_{a-h} = 0.0$ eV/atom [39]) showing its experimental stability, Fig. 1(e). For instance, in Fig. 1(f), Pd_2HgSe_3 lies in a convex node with a formation energy of -0.18 eV/atom. Additionally, all M_2HgSe_3 ($M=Ni, Pd, Pt$) have $E_{a-h} = 0.0$, as well as Pd_2HgTe_3 , Pt_2CdTe_3 and Pt_2HgTe_3 . For the Se and Te based materials that have non-zero energy above hull we found $E_{a-h} < 0.18$ eV/atom, which indicate its high stability [40]. For instance, taking Pt_2ZnTe_3 as a case of study [$E_{a-h} = 0.08$ eV/atom], we have calculated its monolayer phonon dispersion [39], where its dynamical stability was confirmed by the absence of negative frequencies. Additionally, for the higher E_{a-h} systems, $X=S$ based compounds, their negative values of formation energies, $\Omega < 0$ [39], indicates that they can be experimentally stabilized throughout specific synthesis routes and/or substrate support. Although the SOC has a stabilizing role in the jacutingaite phonon dispersion [26], we see that it changes the formation energy by ~ 7 meV/atoms which do not change our conclusions.

The cleavage energy (δ) [41] is another important structural information for the top-down synthesis of 2D systems. We found that the M_2NX_3 bulk phase presents cleavage energies in the range of other experimentally exfoliated materials [42]. For instance, jacutingaite has a cleavage energy ($\delta = 0.46$ J/m²) comparable with that of graphene exfoliated from graphite, $\delta = 0.39$ J/m² [dashed line in Fig. 1(g)] [43]. Comparing the calculated cleavage energy and the vertical buckling of the $N-M-N$ bonds [d_z in Fig. 1(c)] it is noticeable that, (i) for a given transition metal pair $M-N$ the δ is proportional to d_z , being larger for $X=S$ and lower for $X=Te$, it is in agreement with Ref. [32], where the authors verified that the N atoms are responsible for the inter-plane bound of the M_2NX_3 system, as shown in Fig. 1(a) M_2NX_3 3D structure. Indeed, taking the Cd and Hg systems, which

have a similar buckling distance, the former presents a stronger interlayer bond ruled by the bonding energy of Cd- X being $\sim 60\%$ greater than Hg- X . By contrast, for Zn, given its lower buckling distance, an interplay between the vdW interaction (of the TMD host) and the Zn interlayer chemical bond is present. Here the later dominating for lower d_z and leading to weaker interlayer bond. (ii) For $X=\text{Te}$ and $N=\text{Zn}$, the cleavage energy are always lower than that of graphene, where (iii) the cleavage energy of Pt_2HgTe_3 is lower when compared with its counterpart (Pt_2HgSe_3) jacutingaite.

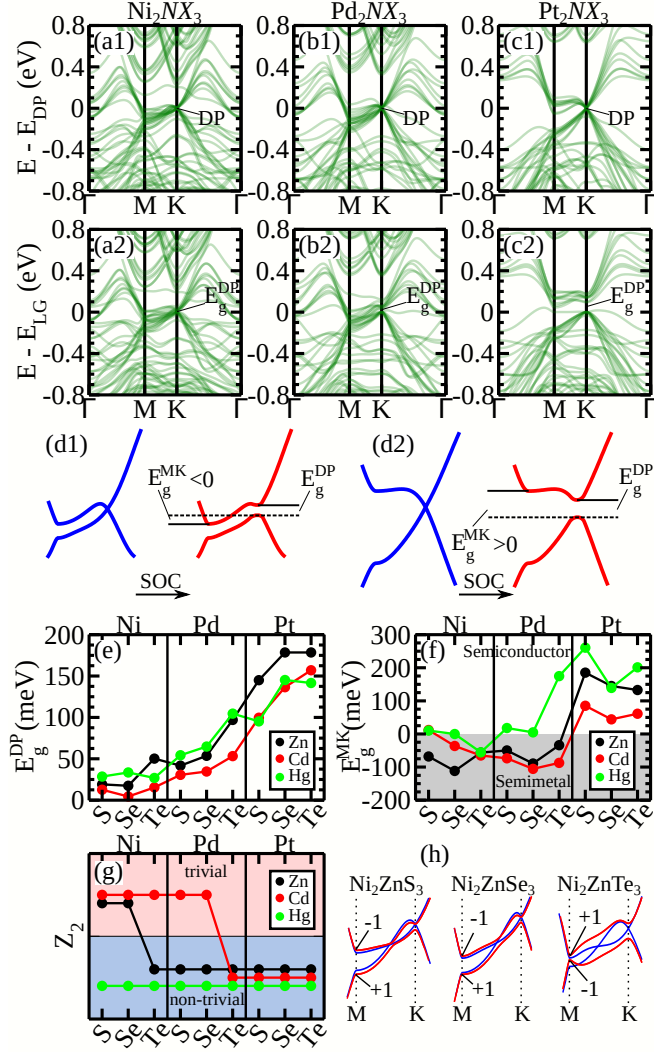


FIG. 2. Superposition of band structures for the (a) Ni_2NX_3 , (b) Pd_2NX_3 and (c) Pt_2NX_3 systems, (a1)-(c1) without SOC and energy in relation to the DP (E_{DP}) and (a2)-(c2) with SOC and energy in relation to the K point gap's lower band (E_{LG}). (d) Depiction of the Dirac bands and SOC effect in the (d1) downward band bending at M and (d2) graphene-like. (e) Dirac point SOC energy gap (E_g^{DP}); (f) global energy gap between M and K points (E_g^{MK}); (g) topological invariant; and (h) topological transition for Ni_2ZnX_3 with blue (red) lines indicating the states without (with) SOC.

Once we have shown the feasibility of the energetically stable counterparts of jacutingaite, here we will focus on the electronic properties and topological phases of single layer $M_2\text{NX}_3$ systems. As shown in Fig. 2(a)-(c), we found the emergence of Dirac cones ruled by the hexagonal $N-M-N$ buckled lattice. The projection of the energy bands, near the Fermi level, reveals that the Dirac cones are mostly composed by the transition metal $N(s)$ orbitals hybridized with the host $M(d)$, orbitals *viz.*: Ni($3d$), Pd($4d$), and Pt($5d$). It is noticeable that, for a given host transition metal M , the electronic band structures share nearly the same features around the Fermi level. For instance, in Fig. 2(a) we present the superposition of the electronic band structures of Ni_2NX_3 with $N=\text{Zn}$, Cd, and Hg, and $X=\text{S}$, Se, and Te; similarly for Pd_2NX_3 and Pt_2NX_3 , as shown in Figs. 2(b) and (c). Such figure, where each material contributes with a translucent set of lines (band structure), allow us to identify similar features in the compounds characterized by darker regions (more details at supplemental material [39]). In the absence of SOC, the linear dispersion of the energy bands at the K and K' gives rise to the Dirac points (DPs) indicated as DP in Figs. 2 panels (a1)-(c1). Whereas, by turning on the SOC contribution, we find energy gaps taking place at the DPs [E_g^{DP} in Fig. 2 panels (a2)-(c2)]. The SOC in the system are most given by the M atoms [26], and its strength is a quantitative indication of the stability of topological states. Here, it is worth to highlight that SOC induced energy gaps at the DP [Fig 2(e)] are larger in Pt_2ZnX_3 compared with the ones of the other Pt_2NX_3 systems. For instance, Pt_2ZnX_3 (with $X=\text{Se}$ or Te) presents $E_g^{\text{DP}} \approx 178$ meV, being larger by 34 meV (23%) compared with that of jacutingaite and its counterpart Pt_2HgTe_3 , both systems present $E_g^{\text{DP}} = 145$ meV. In particular, these findings can be understood by comparing the equilibrium geometries of the $N\text{-Pt-N}$ buckled hexagonal lattice; namely Zn-Pt-Zn presents lower values of vertical buckling and Zn-Pt equilibrium bond length ($d_{MN} = 2.55$ Å) compared with the ones of Hg-Pt-Hg, $d_{MN} = 2.79$ Å, strengthening the Pt contribution to the Zn(s) Dirac bands. It is worth pointing out that larger values of E_g^{DP} in Pt_2ZnX_3 have been maintained even upon the use of hybrid functionals (HSE). Here we found $E_g^{\text{DP}} = 232$ and 242 meV for $X=\text{Se}$ and Te , both larger than that obtained for jacutingaite, 222 meV (in Ref. [44] the authors obtained 218 meV using the same calculation approach).

Besides the energy gap induced by the SOC at the K/K' points, downward bending of the upper Dirac band along the K-M direction leads to lower values of global gaps, and eventually resulting in semimetallic systems. In Fig. 2(f) we show the energy difference between the lower point of the upper Dirac band at the M-point and the top of the Dirac valence band at K-point [E_g^{MK} in Figs. 2(d1)-(d2)]. Negative values of E_g^{MK} , for $M=\text{Ni}$ and Pd systems, indicate that they are semimetallic. For

$M = \text{Pt}$, the SOC strength always overcome the downward band bending, where the semiconducting character has been preserved. Focusing on the Pt_2NTe_3 systems, we found indirect energy band-gaps of 133 and 61 meV for $N = \text{Zn}$ and Hg , respectively, while Pt_2HgTe_3 presents a direct energy gap ($E_g^{\text{DP}} < E_g^{\text{MK}}$) of 142 meV.

To characterize the topological phase of the M_2NX_3 systems we have computed the Z_2 [45] invariant by analyzing the parity of each band at the time-reverse invariant momenta (TRIM) and considering all bands below the upper Dirac bands fully occupied [46]. It is worth noting that the presence of semimetallic bands does not necessarily rule out the (possible) emergence of topologically non-trivial phases, characterizing a Z_2 -metallic phase [47]. In this case, the edge states are no longer protected against backscattering processes. Our results, summarized in Fig. 2(g), reveal that while all Hg compounds present a non-trivial topological phase, Ni_2ZnX_3 and Pd_2CdX_3 systems present a trivial \rightarrow non-trivial topological transition for $X = \text{S} \rightarrow \text{Te}$. In these systems, there is an extra crossing of the Dirac bands (without SOC) along the M–K path [blue lines in Fig. 2(h)], which causes a parity inversion from the original graphene-like bands. Such an inversion is overcome by the SOC, changing the parity order at the TRIM, for $X = \text{Te}$ leading to the Z_2 non-trivial topological phase, whereas in Ni_2ZnX_3 the strength of the SOC is not enough to re-invert this extra crossing.

In addition to the topological phase control (trivial \leftrightarrow non-trivial), as a function of the chemical composition in M_2NX_3 jacutingaite like structures; other properties worth to be examined in order to achieve technological applications, as well as the integration with other 2D materials. For instance, the behavior of the SOC (non-trivial) energy gap as a function of the mechanical strain. Here, we found that the topological phase of the M_2NX_3 jacutingaite like systems are robust against biaxial strain. In particular, for Pt_2ZnSe_3 , there is an increase of the SOC induced non-trivial energy band-gaps, E_g^{DP} , from 178 to 185 meV upon a compressive strain of 2%. It reaches to ~ 194 meV in Pt_2ZnTe_3 compressed by 2.5%. Another key feature, in order to perform electronic engineering based on M_2NX_3 2D heterostructures [48], is the work function (Φ). By examining its dependence with the chemical composition, we found that for a given MX_2 host, Φ varies as a function of the foreign transition metal N . For instance, considering the PtSe_2 host, we found $\Phi = 4.90$ eV for jacutingaite ($N = \text{Hg}$), and it increases to about 4.70 eV in Pt_2ZnSe_3 . Meanwhile, in Pt_2NTe_3 Φ reduces to 4.73 and 4.43 eV for $N = \text{Hg}$ and Zn , respectively. Further details of the SOC induced bandgap as a function of biaxial strain and M_2NX_3 work functions are shown in the supplemental material [39].

In conclusion, we have shown that beyond the jacutingaite, which is a naturally occurring mineral, there are other jacutingaite like (M_2NX_3) structures that also

host the Kane-Mele QSH phase. The energetic stability of these M_2NX_3 jacutingaite counterparts was thoroughly investigated, based on formation energy calculations combined with the recently convex hull analysis. We found that the M_2NX_3 structures are quite stable for chalcogenide (X) Se and Te atoms. Further calculations of the cleavage energies show that these systems can be isolated in monolayers by commonly used exfoliation methods. The topological phases were characterized upon the calculation of Z_2 and Z_2 -metallic invariants, where we found that for $N = \text{Hg}$ the non-trivial phase has been preserved for any combination between the transition metal M ($= \text{Ni}$, Pd , and Pt) and chalcogenide atom X ($= \text{S}$, Se , and Te). In contrast, for the other foreign transition metals, $N = \text{Zn}$ and Cd , the topological phase depends on the combination of the host (MX_2) atoms. Finally, we found that the Zn compounds, Pt_2ZnSe_3 and Pt_2ZnTe_3 , present larger values of topological bandgap compared with that of jacutingaite (Pt_2HgSe_3), while by changing the host element, $X = \text{Se} \rightarrow \text{Te}$, the bandgap is practically the same, however, it becomes direct. Nevertheless, the unveiled class of materials introduces a family of compounds hosting the Kane-Mele topological phase, which can be of interest in devices engineering.

The authors acknowledge financial support from the Brazilian agencies FAPESP (grants 19/20857-0 and 17/02317-2), CNPq, and FAPEMIG, and the CENAPAD-SP and Laboratório Nacional de Computação Científica (LNCC-SCAFMat2) for computer time.

* felipe.lima@lnnano.cnpem.br

† hiroki@ufu.br

‡ adalberto.fazzio@lnnano.cnpem.br

- [1] M. Z. Hasan and C. L. Kane, “Colloquium: Topological insulators,” *Rev. Mod. Phys.* **82**, 3045–3067 (2010).
- [2] Carlos Mera Acosta, Elton Ogoshi, Adalberto Fazzio, Gustavo M. Dalpian, and Alex Zunger, “The Rashba Scale: Emergence of Band Anti-crossing as a Design Principle for Materials with Large Rashba Coefficient,” *Matter* **3**, 145 – 165 (2020).
- [3] L. L. Tao and Evgeny Y. Tsymbal, “Persistent spin texture enforced by symmetry,” *Nature Communications* **9**, 2763 (2018).
- [4] Xiaoqing Liang, Xue Wu, Jun Hu, Jijun Zhao, and Xiao Cheng Zeng, “Large magnetic anisotropy in chemically engineered iridium dimer,” *Communications Physics* **1**, 74 (2018).
- [5] Miao Jiang, Hirokatsu Asahara, Shoichi Sato, Toshiki Kanaki, Hiroki Yamasaki, Shinobu Ohya, and Masaaki Tanaka, “Efficient full spin-orbit torque switching in a single layer of a perpendicularly magnetized single-crystalline ferromagnet,” *Nature Communications* **10**, 2590 (2019).
- [6] K. S. Novoselov, A. K. Geim, S. V. Morozov, D. Jiang, Y. Zhang, S. V. Dubonos, I. V. Grigorieva, and A. A.

- Firsov, “Electric Field Effect in Atomically Thin Carbon Films,” *Science* **306**, 666–669 (2004).
- [7] Ethan C. Ahn, “2D materials for spintronic devices,” *npj 2D Materials and Applications* **4**, 17 (2020).
- [8] Kasun Premasiri and Xuan P A Gao, “Tuning spin-orbit coupling in 2D materials for spintronics: a topical review,” *Journal of Physics: Condensed Matter* **31**, 193001 (2019).
- [9] A. Avsar, H. Ochoa, F. Guinea, B. Özyilmaz, B. J. van Wees, and I. J. Vera-Marun, “Colloquium: Spintronics in graphene and other two-dimensional materials,” *Rev. Mod. Phys.* **92**, 021003 (2020).
- [10] C. L. Kane and E. J. Mele, “Quantum Spin Hall Effect in Graphene,” *Phys. Rev. Lett.* **95**, 226801 (2005).
- [11] Chen Si, Kyung-Hwan Jin, Jian Zhou, Zhimei Sun, and Feng Liu, “Large-Gap Quantum Spin Hall State in MXenes: d-Band Topological Order in a Triangular Lattice,” *Nano Letters* **16**, 6584–6591 (2016).
- [12] Nathan C. Frey, Hemant Kumar, Babak Anasori, Yury Gogotsi, and Vivek B. Shenoy, “Tuning Noncollinear Spin Structure and Anisotropy in Ferromagnetic Nitride MXenes,” *ACS Nano* **12**, 6319–6325 (2018).
- [13] Wei-xiao Ji, Chang-wen Zhang, Meng Ding, Ping Li, and Pei-ji Wang, “Quantum spin Hall phase transitions in two-dimensional SbBi alloy films,” *J. Mater. Chem. C* **5**, 2649–2655 (2017).
- [14] F. Reis, G. Li, L. Dudy, M. Bauernfeind, S. Glass, W. Hanke, R. Thomale, J. Schäfer, and R. Claessen, “Bismuthene on a SiC substrate: A candidate for a high-temperature quantum spin Hall material,” *Science* **357**, 287–290 (2017).
- [15] Sobhit Singh and Aldo H. Romero, “Giant tunable Rashba spin splitting in a two-dimensional BiSb monolayer and in BiSb/AlN heterostructures,” *Phys. Rev. B* **95**, 165444 (2017).
- [16] Conan Weeks, Jun Hu, Jason Alicea, Marcel Franz, and Ruqian Wu, “Engineering a Robust Quantum Spin Hall State in Graphene via Adatom Deposition,” *Phys. Rev. X* **1**, 021001 (2011).
- [17] Hongbin Zhang, Cesar Lazo, Stefan Blügel, Stefan Heinze, and Yuriy Mokrousov, “Electrically Tunable Quantum Anomalous Hall Effect in Graphene Decorated by 5d Transition-Metal Adatoms,” *Phys. Rev. Lett.* **108**, 056802 (2012).
- [18] C. Mera Acosta, Matheus P. Lima, R. H. Miwa, Antônio J. R. da Silva, and A. Fazzio, “Topological phases in triangular lattices of Ru adsorbed on graphene: Ab initio calculations,” *Phys. Rev. B* **89**, 155438 (2014).
- [19] Ilya I. Klimovskikh, Mikhail M. Otrokov, Vladimir Yu. Voroshnin, Daria Sostina, Luca Petaccia, Giovanni Di Santo, Sangeeta Thakur, Evgueni V. Chulkov, and Alexander M. Shikin, “Spin–Orbit Coupling Induced Gap in Graphene on Pt(111) with Intercalated Pb Monolayer,” *ACS Nano* **11**, 368–374 (2017).
- [20] Amir Muhammad Afzal, Kuen Hong Min, Byung Min Ko, and Jonghwa Eom, “Observation of giant spin–orbit interaction in graphene and heavy metal heterostructures,” *RSC Adv.* **9**, 31797–31805 (2019).
- [21] T. Wakamura, F. Reale, P. Palczynski, M. Q. Zhao, A. T. C. Johnson, S. Guéron, C. Mattevi, A. Ouerghi, and H. Bouchiat, “Spin-orbit interaction induced in graphene by transition metal dichalcogenides,” *Phys. Rev. B* **99**, 245402 (2019).
- [22] Zhenhua Qiao, Wei Ren, Hua Chen, L. Bellaiche, Zhenyu Zhang, A. H. MacDonald, and Qian Niu, “Quantum Anomalous Hall Effect in Graphene Proximity Coupled to an Antiferromagnetic Insulator,” *Phys. Rev. Lett.* **112**, 116404 (2014).
- [23] Zhiyong Wang, Chi Tang, Raymond Sachs, Yafis Barlas, and Jing Shi, “Proximity-Induced Ferromagnetism in Graphene Revealed by the Anomalous Hall Effect,” *Phys. Rev. Lett.* **114**, 016603 (2015).
- [24] J. B. S. Mendes, O. Alves Santos, L. M. Meireles, R. G. Lacerda, L. H. Vilela-Leão, F. L. A. Machado, R. L. Rodríguez-Suárez, A. Azevedo, and S. M. Rezende, “Spin-Current to Charge-Current Conversion and Magnetoresistance in a Hybrid Structure of Graphene and Yttrium Iron Garnet,” *Phys. Rev. Lett.* **115**, 226601 (2015).
- [25] A. R. Cabral, H. F. Galbiatti, R. Kwitko-Ribeiro, and B. Lehmann, “Platinum enrichment at low temperatures and related microstructures, with examples of hongshilite (PtCu) and empirical ‘Pt₂HgSe₃’ from Itabira, Minas Gerais, Brazil,” *Terra Nova* **20**, 32–37 (2008).
- [26] Antimo Marrazzo, Marco Gibertini, Davide Campi, Nicolas Mounet, and Nicola Marzari, “Prediction of a Large-Gap and Switchable Kane-Mele Quantum Spin Hall Insulator,” *Phys. Rev. Lett.* **120**, 117701 (2018).
- [27] Jorge I. Facio, Sanjib Kumar Das, Yang Zhang, Klaus Koepf, Jeroen van den Brink, and Ion Cosma Fulga, “Dual topology in jacutingaite Pt₂HgSe₃,” *Phys. Rev. Materials* **3**, 074202 (2019).
- [28] Barun Ghosh, Sougata Mardanya, Bahadur Singh, Xiaoting Zhou, Baokai Wang, Tay-Rong Chang, Chenliang Su, Hsin Lin, Amit Agarwal, and Arun Bansil, “Saddlepoint Van Hove singularity and dual topological state in Pt₂HgSe₃,” *Phys. Rev. B* **100**, 235101 (2019).
- [29] Antimo Marrazzo, Nicola Marzari, and Marco Gibertini, “Emergent dual topology in the three-dimensional Kane-Mele Pt₂HgSe₃,” *Phys. Rev. Research* **2**, 012063 (2020).
- [30] Konrád Kandrai, Péter Vancsó, Gergő Kukucska, János Koltai, György Baranka, Ákos Hoffmann, Áron Pekker, Katalin Kamarás, Zolt E. Horváth, Anna Vymazalová, Levente Tapasztó, and Péter Nemes-Incze, “Signature of Large-Gap Quantum Spin Hall State in the Layered Mineral Jacutingaite,” *Nano Letters* **20**, 5207–5213 (2020).
- [31] I. Cucchi, A. Marrazzo, E. Cappelli, S. Riccò, F. Y. Bruno, S. Lisi, M. Hoesch, T. K. Kim, C. Cacho, C. Besnard, E. Giannini, N. Marzari, M. Gibertini, F. Baumberger, and A. Tamai, “Bulk and Surface Electronic Structure of the Dual-Topology Semimetal Pt₂HgSe₃,” *Phys. Rev. Lett.* **124**, 106402 (2020).
- [32] Anna Vymazalová, Frantisek Laufek, Milan Drábek, Alexandre R. Cabral, Jakub Haloda, Tamara Sidorinová, Bernd Lehmann, Henry F. Galbiatti, and Jan Drahoš, “Jacutingaite, Pt₂HgSe₃, a new platinum-group mineral species from the Cauê iron-ore deposit, Itabira district, Minas Gerais, Brazil,” *The Canadian Mineralogist* **50**, 431–440 (2012).
- [33] Raphael Longuinhos, Anna Vymazalová, Alexandre R. Cabral, Simone S. Alexandre, Ricardo W. Nunes, and Jenaina Ribeiro-Soares, “Raman spectrum of layered jacutingaite (Pt₂HgSe₃) crystals—Experimental and theoretical study,” *Journal of Raman Spectroscopy* **51**, 357–365 (2020).
- [34] F. Laufek, A. Vymazalová, and M. Drábek, “Powder diffraction study of Pd₂HgSe₃,” *Powder Diffraction* **32**,

- 244–248 (2017).
- [35] See supplemental materials at <http://XXX> for the computational details citing references [49–57].
- [36] Shyue Ping Ong, Lei Wang, Byoungwoo Kang, and Gerbrand Ceder, “Li-Fe-P-O2 Phase Diagram from First Principles Calculations,” *Chemistry of Materials* **20**, 1798–1807 (2008).
- [37] Shyue Ping Ong, Anubhav Jain, Geoffroy Hautier, Byoungwoo Kang, and Gerbrand Ceder, “Thermal stabilities of delithiated olivine MPO4 (M=Fe, Mn) cathodes investigated using first principles calculations,” *Electrochemistry Communications* **12**, 427 – 430 (2010).
- [38] Anubhav Jain, Shyue Ping Ong, Geoffroy Hautier, Wei Chen, William Davidson Richards, Stephen Dacek, Shreyas Cholia, Dan Gunter, David Skinner, Gerbrand Ceder, and Kristin A. Persson, “Commentary: The Materials Project: A materials genome approach to accelerating materials innovation,” *APL Materials* **1**, 011002 (2013).
- [39] See supplemental materials at <http://XXX> for (i) ternary phase diagram, (ii) phonon dispersion of Pt₂ZnTe₃, (iii) detailed band structures, (iv) strain effect on the SOC gap and (v) work function.
- [40] Gabriel R. Schleder, Carlos Mera Acosta, and Adalberto Fazzio, “Exploring Two-Dimensional Materials Thermodynamic Stability via Machine Learning,” *ACS Applied Materials & Interfaces* **12**, 20149–20157 (2020).
- [41] $\delta = (E_{bulk} - E_{ML})/A$, with E_{bulk} (E_{ML}) the total energy of the bulk (monolayer) system, and A monolayer the unity cell area.
- [42] Kamal Choudhary, Irina Kalish, Ryan Beams, and Francesca Tavazza, “High-throughput Identification and Characterization of Two-dimensional Materials using Density functional theory,” *Scientific Reports* **7**, 5179 (2017).
- [43] Wen Wang, Shuyang Dai, Xide Li, Jiarui Yang, David J. Srolovitz, and Quanshui Zheng, “Measurement of the cleavage energy of graphite,” *Nature Communications* **6**, 7853 (2015).
- [44] Xianxin Wu, Mario Fink, Werner Hanke, Ronny Thomale, and Domenico Di Sante, “Unconventional superconductivity in a doped quantum spin Hall insulator,” *Phys. Rev. B* **100**, 041117 (2019).
- [45] C. L. Kane and E. J. Mele, “Z₂ Topological Order and the Quantum Spin Hall Effect,” *Phys. Rev. Lett.* **95**, 146802 (2005).
- [46] Liang Fu and C. L. Kane, “Topological insulators with inversion symmetry,” *Phys. Rev. B* **76**, 045302 (2007).
- [47] Bao Zhao, Jiayong Zhang, Wanxiang Feng, Yugui Yao, and Zhongqin Yang, “Quantum spin Hall and Z₂ metallic states in an organic material,” *Phys. Rev. B* **90**, 201403 (2014).
- [48] A. K. Geim and I. V. Grigorieva, “Van der Waals heterostructures,” *Nature* **499**, 419–425 (2013).
- [49] G. Kresse and J. Furthmüller, “Efficiency of ab-initio total energy calculations for metals and semiconductors using a plane-wave basis set,” *Computational Materials Science* **6**, 15 – 50 (1996).
- [50] J. P. Perdew, K. Burke, and M. Ernzerhof, “Generalized gradient approximation made simple,” *Phys. Rev. Lett.* **77**, 3865 (1996).
- [51] Jochen Heyd, Gustavo E. Scuseria, and Matthias Ernzerhof, “Hybrid functionals based on a screened Coulomb potential,” *The Journal of Chemical Physics* **118**, 8207–8215 (2003).
- [52] Jochen Heyd, Gustavo E. Scuseria, and Matthias Ernzerhof, “Erratum: “hybrid functionals based on a screened coulomb potential” [j. chem. phys. 118, 8207 (2003)],” *The Journal of Chemical Physics* **124**, 219906 (2006).
- [53] Hendrik J. Monkhorst and James D. Pack, “Special points for Brillouin-zone integrations,” *Phys. Rev. B* **13**, 5188–5192 (1976).
- [54] P. E. Blöchl, “Projector augmented-wave method,” *Phys. Rev. B* **50**, 17953–17979 (1994).
- [55] Kyuho Lee, Éamonn D. Murray, Lingzhu Kong, Bengt I. Lundqvist, and David C. Langreth, “Higher-accuracy van der waals density functional,” *Phys. Rev. B* **82**, 081101 (2010).
- [56] Laurent Chaput, Atsushi Togo, Isao Tanaka, and Gilles Hug, “Phonon-phonon interactions in transition metals,” *Phys. Rev. B* **84**, 094302 (2011).
- [57] Atsushi Togo and Isao Tanaka, “First principles phonon calculations in materials science,” *Scripta Materialia* **108**, 1 – 5 (2015).